The combined effects of water saturation and strain rate on crack initiation and damage stress of rock

Jun Zhu
Key Laboratory of Mountain Hazards and Earth Surface Process, Institute of Mountain Hazards and Environment, Chinese Academy of Sciences (CAS), Chengdu, Sichuan, China

Jianhui Deng
State Key Laboratory of Hydraulics and Mountain River Engineering, College of Water Resources and Hydropower, Sichuan University, Chengdu, Sichuan, China

ABSTRACT: Here, we reported a series of uniaxial compression and acoustic emission (AE) tests performed on dry and saturated marble at different strain rates, which offer new information on the combined effects of water saturation and strain rate on its crack initiation CI stress and crack damage CD stress. The test data show that the water saturation causes various reductions in the ratio of CI stress to peak stress N_{CI}, while increments in the ratio of CD stress to peak stress N_{CD}. This N_{CI} reduction is due to the main water-weakening effect of pore water pressure, and the increase in N_{CD} is caused by the additional vicious effect. The N_{CI} of saturated marble shows a decreasing trend with increasing strain rates, while that of N_{CD} remains nearly constant. By easily initiating more small defects, the strain rate effect can strengthen the N_{CI} reduction and inhibit the N_{CD} increase.

Keywords: stress threshold; water saturation; strain rate; acoustic emission; dominant frequency.

1 INTRODUCTION

The International Society for Rock Mechanics and Rock Engineering (ISRM) has proposed two typical stress thresholds according to rock crack propagation activity: the crack initiation (CI) threshold and the crack damage (CD) threshold, as depicted in Figure 1. Accordingly, the axial stress corresponding to the CI and CD thresholds are referred to as CI stress and CD stress, respectively. In particular, CI stress indicates the applied stress at which these cracks begin to nucleate, and CD stress represents the onset of shear deformation owing to microcrack coalescence (Diederichs & Martin, 2010). CI and CD stress can be determined using several methods and testing procedures, such as the axial/lateral strain method (Lajtai, 1974), volumetric strain method (Brace et al., 1966), crack volumetric strain method (Martin & Chandler, 1994), moving point regression method (Eberhardt et al., 1998), and acoustic emission (AE) method (Ranjith et al., 2010; Zhao et al., 2013). These methods depend more or less on the user's subjective judgments and thus compromise the accuracy of stress thresholds determination. Hence, a reliable method with explicit physical meaning would benefit the determination of CI and CD stress thresholds.

Most of the rock masses are soaking in environments formed by various water sources, e.g., groundwater, pore water, precipitation, and water impounded in reservoirs. It is widely recognized that water saturation has drastic effects on the rock crack propagation process, facilitating rock weakening and deterioration (Erguler & Ulusay, 2009; Shimbo et al., 2022). Moreover, loads characterized by various rates can be superimposed on saturated rock mass. The loading rate or strain rate is believed closely related to the extent of rock rupture and crack propagation (Wasantha et al., 2014). It means that the water saturation and strain rate have combined effects on rock crack development, thus making the CI and CD stress vary. To date, despite limited efforts devoted to investigating the crack stress thresholds of saturated rocks (Yao et al., 2016; Zhu et al., 2019a), the combined effects of water saturation and strain rate on rock crack stress thresholds remain unclear. Two main reasons can explain such a dilemma: 1) multiple water-weakening mechanisms that arose together make it difficult to quantify their extent, and 2) the rock fracture affected by strain rate can not be quantitatively characterized. In other words, a comprehensive understanding of the combined effects of water saturation and strain rate on crack stress thresholds is lacking due to the absence of a reliable quantitative analysis method.

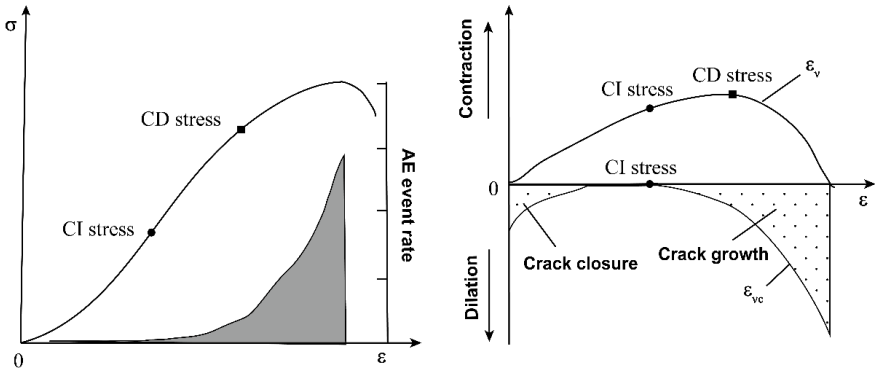

Figure 1. The determination of crack stress thresholds.

In this work, detailed experimental procedures were presented to investigate the combined effects of water saturation and strain rate on the CI and CD stress thresholds of marble rock by static compression tests. In particular, the dominant frequencies of AE waveforms released in the vicinity of crack stress thresholds were extracted to interpret the variation of CI and CD stress using a novel statistical analysis method.

2 EXPERIMENTAL PROCEDURES

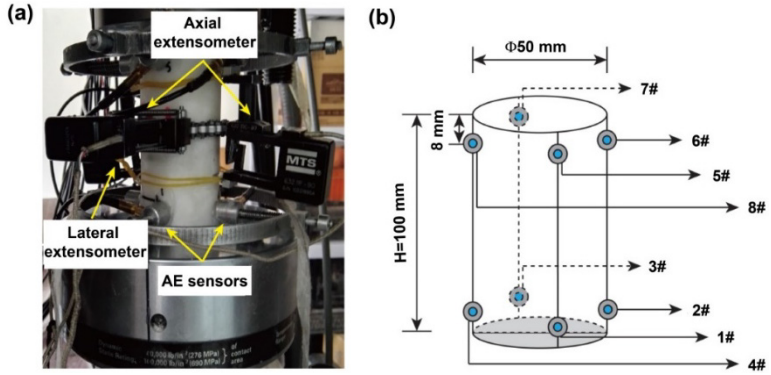

Figure 2. Loading setup for rock samples at different strain rates, (a) loading sample, (b) AE sensors layout.

All marble specimens were cored from a single block, which is constituted by calcite mineral only, as confirmed by the X-ray diffraction (XRD) measurement. These specimens were fabricated into

standard cylinders with a size of H100 mm×Φ50 mm. Herein, all samples were firstly dehydrated in a vacuum oven at 105 °C for 48 h, and half of them were cooled down to prepare the dry samples. The rest were then soaked in distilled water for 48 h inside a vacuum chamber (pressure: -0.1 MPa) and were left to stand for 4 h (Zhu et al., 2022). The saturated samples were ready when the full saturation state was reached using multiple weighing.

The static compressive experiments were performed with a rock loading apparatus (MTS 815) and an AE monitoring system (PCI-2). A linear variable differential transformer (LVDT) with an accuracy of 0.1% was used to measure the axial displacement and thus control the applied strain rate during the tests. Specifically, the axial and lateral displacements of the sample were measured by the axial extensometer and lateral extensometer (see Figure 2), respectively. The applied strain rates were 1.67×10^{-6}, 8.33×10^{-6}, 1.67×10^{-5}, 8.33×10^{-5} and 1.67×10^{-4} s^{-1}. As shown in Figure 2, the sample was equipped with eight micro30 sensors symmetrically in the radial direction along the surface. The pre-amplification was set as 40 dB, and the sampling frequency was 1 MHz.

3 EXPERIMENTAL RESULTS AND DISCUSSION

3.1 Crack stress thresholds determination

Given the performance of a reliable mathematical process, the volumetric strain and crack volumetric strain methods are expected to be reasonable to determine crack stress thresholds as indicated by our previous studies (Zhu et al., 2019b). Hence, the volumetric strain and crack volumetric strain curves are used to identify the crack stress thresholds in this study. In particular, the CI stress corresponds to the stress at the end of the horizontal section with a crack volumetric strain of zero, while the CD stress corresponds to the stress at the inflection point of the volumetric strain curve. Note that, a range of volumetric strain data including the inflection point is fitted and the analytical solution of the inflection point is then obtained using the Matlab program. As shown in Figure 3, the CI stress for dry and saturated samples (points B and D) are determined as 21.41 and 14.73 MPa, and the CD stress of them (points A and C) are 43.63 and 38.16 MPa, respectively.

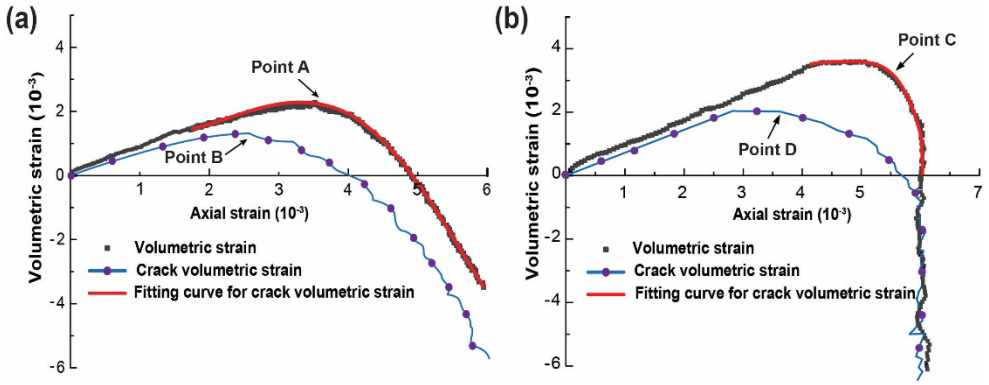

Figure 3. The determination of CI and CD stress for typical samples, (a) dry sample, (b) saturated sample.

3.2 Effects of strain rates and water saturation

Figure 4 shows the variations of normalized CI stress N_{CI} and normalized CD stress N_{CD} of rock samples. The normalized crack stress, i.e, N_{CI} and N_{CD}, is defined as the ratio of crack stress, i.e., CI stress and CD stress, to the peak stress, respectively. For the tested marble under both dry and water-saturated conditions, the N_{CI} was a decreasing function of the strain rates. Water-saturated samples were characterized by lower N_{CI} than dry samples. Indeed, the N_{CI} under water-saturated conditions was 7.84, 6.57, 4.88, 4.14, and 5.72% lower than those under dry conditions as the strain rates increased from 1.67×10^{-6} to 1.67×10^{-4} s^{-1}. Regarding the N_{CD}, the values obtained for dry marble gradually decreased with increasing strain rates, while that of saturated marble was kept almost constant. Additionally, the N_{CD} of water-saturated samples was generally greater than that

of dry samples. In particular, the N_{CI} under water-saturated conditions was 1.51, 9.84, 12.82, 14.02, and 16.23% greater than under dry conditions when the strain rates increased from 1.67×10^{-6} to 1.67×10^{-4} s^{-1}. These findings indicate that water saturation causes a considerable reduction in the N_{CI} , but an increase in the N_{CD}, and the strain rates make the N_{CI} and N_{CD} decrease.

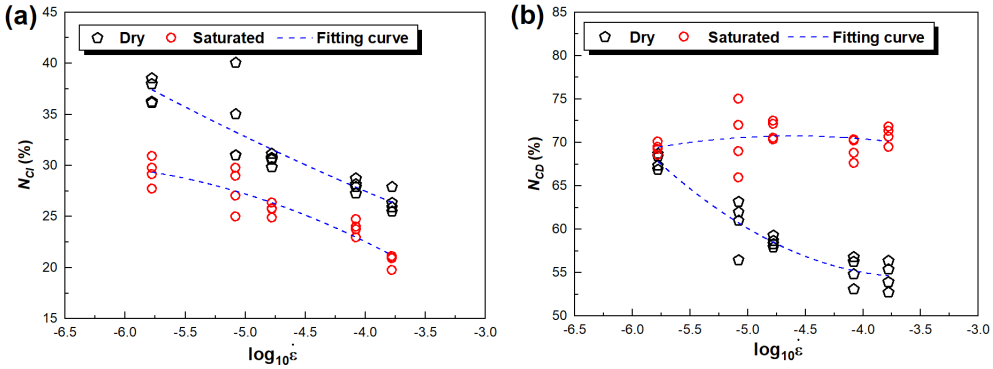

Figure 4. The correlation of crack stress thresholds with strain rates, (a) N_{CI}, (b) N_{CD}.

3.3 Analysis of combined effects based on the dominant frequency of AE waveforms

The dominant frequency of AE waveform signals released during the loading application was extracted using Fast Fourier Transform (FFT). The distribution of the dominant frequency of AE waveforms against the loading time is shown in Figure 5, as well as the applied stress. Based on the crack stress thresholds determined, the dominant frequencies of AE waveform signals located within 10s prior to the corresponding time of the crack stress threshold were selected for the following analysis. Further, these dominant frequencies of AE waveforms were classified into different bands, and the feature of two concentrations was found. In particular, we called the AE waveforms distributed in the two concentrations of dominant frequency bands (i.e., high dominant frequency band and low dominant frequency band) the H-type waveforms and the L-type waveforms. Afterward, the percentages of H-type waveforms and L-type waveforms were calculated. For simplicity, P_{H-CI} and P_{L-CI} indicate the percentage of H-type and L-type waveforms released in the vicinity of the CI stress threshold, and P_{H-CI} and P_{L-CI} represent the percentage of H-type and L-type waveforms released in the vicinity of the CD stress threshold. For more detail about the dominant frequency of AE waveforms classification, the readers could refer to our previous studies, e.g. Zhu et al. (2022) and Zhu et al. (2019a).

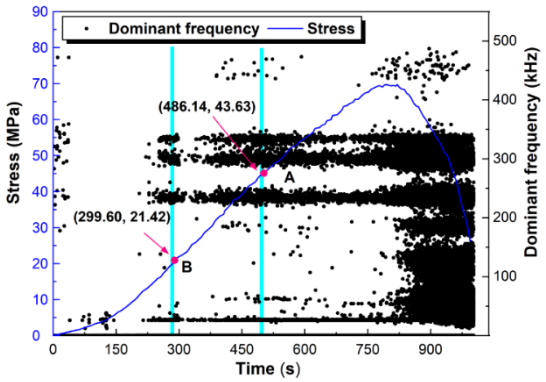

Figure 5. Determining the dominant frequency of AE waveform in the vicinity of CI and CD stress.

Since there is a mutually inhibiting relationship between the percentages of the two types of AE waveforms, the L-type waveforms were used as the representative indicator in this work. As shown in Figure 6, the L-type waveforms dominate all the AE waveforms for saturated marble in the

vicinity of both CI and CD stress thresholds, while that for dry marble is H-type waveforms. It suggests that water saturation results in the generation of more L-type waveforms. For the tested marble under both dry and saturated conditions, the P_{L-CI} is an increasing function of the logarithm of strain rates, and this positive correlation is more pronounced for saturated marble. It indicates that the strain rates cause a slight increase in P_{L-CI}; the combined effects due to the addition of water saturation enhance this increase. However, P_{L-CD} is found to keep constant at varying strain rates for saturated marble. Despite the large data discreteness, the P_{L-CD} of dry marble slightly increases with growing strain rates. It indicates that the strain rate effect causes an increase in both P_{L-CI} and P_{L-CD}, as inferred from the results of dry marble. The combined effects of water saturation and strain rate make the L-type waveforms dominant and enhance the positive correlation of L-type waveform percentage with strain rates.

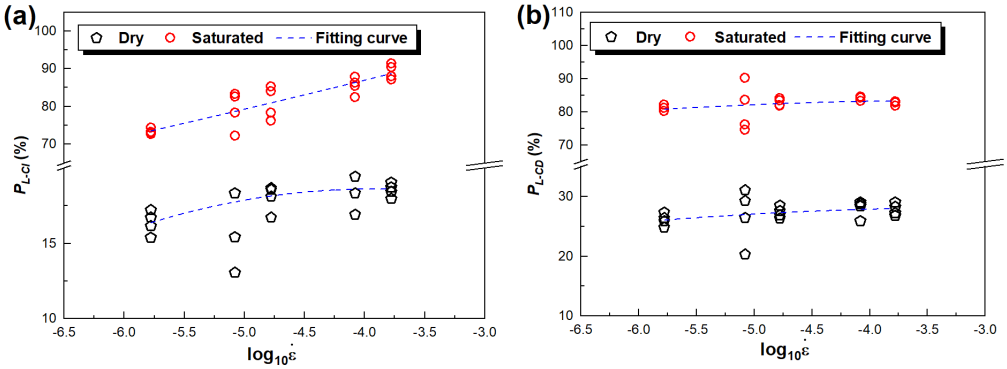

Figure 6. The correlation of P_{L-CI} and P_{L-CD} with strain rates, (a) P_{L-CI}, (b) P_{L-CD}.

The dominant frequency of AE waveforms is a useful indicator for rock failure mode classification (Wang et al., 2019). Further, the results of numerous experiments on different rocks reveal that H-type waveforms are found to be caused by shear failures, and L-type waveforms are expected to produce by tensile failures. With this connection, the reduction in N_{CI} of saturated marble can be attributed to the increase in tensile failures, manifesting the drastic increase in P_{L-CI}. This is because the tensile failures are more easily generated due to the water-weakening effects, e.g., pore water pressure (Zhu et al., 2020). As a result, rock crack initiation is more prone to occur at lower stress levels. However, when rock is undergoing unsteady crack propagation, some water enhancement effects, e.g., the vicious effects, exert due to the fast growth rate and this would inhibit the crack damage stress threshold, as expected. The rock failure modes and delay time of failure generation are both believed to be closely correlative with strain rate (Liang et al., 2015). It is well known that increasing the strain rate activates more defects or failures. This fact supports our conclusions that the N_{CI} and N_{CD} are negative with strain rate and the P_{L-CI} and P_{L-CD} are positive with strain rate. It means that, with increasing strain rates, more failures (represented by tensile failure in this study) are generated and the crack stress thresholds would, of course, become lower. Moreover, since the water-weakening effects (pore water pressure mainly) and water-enhancing effects (vicious mainly) lead to a reduction in N_{CI} and increase in N_{CD}, the extra strain rate effect could enhance the reduction in N_{CI} and inhibit the increase in N_{CD}. This is why, with increasing strain rates, the decrements in N_{CI} for saturated marble increase compared to dry marble, and the N_{CD} for saturated marble trends to keep constant.

4 CONCLUSIONS

The most relevant findings derived from this study are summarized below:

(1) Water saturation causes various normalized CI stress N_{CI} reductions, but normalized CD stress N_{CD} increments at the strain rates investigated. The N_{CI} reduction is due to the main water-weakening effect of pore water pressure, and the increase in N_{CD} is caused by the extra vicious effect.

(2) With increasing strain rates, the N_{CI} and N_{CD} of dry marble both decrease, which is responsible for the easy activation of more small defects derived from the strain rate effect.
(3) The N_{CI} of saturated marble reduces with increasing strain rates, while that of the N_{CD} keeps almost constant. This is due to the strain rate effect can strengthen the N_{CI} reduction and inhibit the N_{CD} increase.

ACKNOWLEDGMENTS

This work was supported by the Second Tibetan Plateau Scientific Expedition and Research Program (STEP) (Grant No. 2019QZKK0904), the National Natural Science Foundation of China (Grant No. U19A2049), and Sichuan Science and Technology Program (2023NSFSC0786).

REFERENCES

Brace, W., Paulding Jr, B., & Scholz, C. 1966. Dilatancy in the fracture of crystalline rocks. Journal of Geophysical Research 71(16), pp.3939-3953.

Diederichs, M., & Martin, C. 2010. Measurement of spalling parameters from laboratory testing. Paper presented at the ISRM International Symposium-EUROCK 2010.

Eberhardt, E., Stead, D., Stimpson, B., & Read, R. 1998. Identifying crack initiation and propagation thresholds in brittle rock. Canadian Geotechnical Journal 35(2), pp.222-233.

Erguler, Z. A., & Ulusay, R. 2009. Water-induced variations in mechanical properties of clay-bearing rocks. International Journal of Rock Mechanics and Mining Sciences 46(2), pp.355-370.

Lajtai, E. 1974. Brittle fracture in compression. International Journal of Fracture 10(4), pp.525-536.

Liang, C., Wu, S., Li, X., & Xin, P. 2015. Effects of strain rate on fracture characteristics and mesoscopic failure mechanisms of granite. International Journal of Rock Mechanics and Mining Sciences (76), pp.146-154.

Martin, C., & Chandler, N. 1994. The progressive fracture of Lac du Bonnet granite. Paper presented at the International Journal of Rock Mechanics and Mining Sciences & Geomechanics Abstracts.

Ranjith, P., Jasinge, D., Choi, S., Mehic, M., & Shannon, B. 2010. The effect of CO2 saturation on mechanical properties of Australian black coal using acoustic emission. Fuel 89(8), pp.2110-2117.

Shimbo, T., Shinzo, C., Uchii, U., Itto, R., & Fukumoto, Y. 2022. Effect of water contents and initial crack lengths on mechanical properties and failure modes of pre-cracked compacted clay under uniaxial compression. Engineering Geology 301, pp.106593.

Wang, Y., Deng, J., Li, L., & Zhang, Z. 2019. Micro-failure Analysis of Direct and Flat Loading Brazilian Tensile Tests. Rock Mechanics and Rock Engineering 52(11), pp.4175-4187. doi:10.1007/s00603-019-01877-7

Wasantha, P. L. P., Ranjith, P. G., Zhao, J., Shao, S. S., & Permata, G. 2014. Strain Rate Effect on the Mechanical Behaviour of Sandstones with Different Grain Sizes. Rock Mechanics and Rock Engineering 48(5), pp.1883-1895. doi:10.1007/s00603-014-0688-4

Yao, Q., Chen, T., Ju, M., Liang, S., Liu, Y., & Li, X. 2016. Effects of Water Intrusion on Mechanical Properties of and Crack Propagation in Coal. Rock Mechanics and Rock Engineering 49(12), pp.4699-4709. doi:10.1007/s00603-016-1079-9

Zhao, X., Cai, M., Wang, J., & Ma, L. 2013. Damage stress and acoustic emission characteristics of the Beishan granite. International Journal of Rock Mechanics and Mining Sciences 64, pp.258-269.

Zhu, J., Deng, J., Chen, F., Huang, Y., & Yu, Z. 2020. Water Saturation Effects on Mechanical and Fracture Behavior of Marble. International Journal of Geomechanics 20(10), pp.04020191. doi:10.1061/(asce)gm.1943-5622.0001825

Zhu, J., Deng, J., Chen, F., & Wang, F. 2022. Failure analysis of water-bearing rock under direct tension using acoustic emission. Engineering Geology 299, pp.106541. doi:10.1016/j.enggeo.2022.106541

Zhu, J., Deng, J., Huang, Y., & He, Z. 2019a. Influence of Water on the Fracture Process of Marble with Acoustic Emission Monitoring. Ksce Journal of Civil Engineering 23(7), pp.3239-3249. doi:10.1007/s12205-019-0172-5

Zhu, J., Deng, J., Huang, Y., & Yu, Z. 2019b. Experimental study on characteristic strength of saturated marble. Chinese Journal of Rock Mechanics and Engineering 38(6), pp.1129-1138.